Resolving the Rise and Fall of Star Formation in Galaxies
Proceedings IAU Symposium No. 373, 2023
T. Wong & W.-T. Kim, eds.
doi:10.1017/S1743921322003684

Molecular Clouds with CO-dark Envelopes in the Extended Ultraviolet (XUV) Disk of M83

Jin Koda

Department of Physics and Astronomy, Stony Brook University, Stony Brook, NY 11794-3800

Abstract. We report a CO(3-2) detection of 23 molecular clouds in the extended ultraviolet (XUV) disk of the spiral galaxy M83 with ALMA. The observed 1 kpc^2 region is at about $1.24R_{25}$ from the disk center, where CO(2-1) was previously not detected. The detection and non-detection, as well as the level of star formation (SF) activity in the region, can be explained consistently if the clouds have the mass distribution common among Galactic clouds, such as Orion A – with star-forming dense clumps embedded in thick layers of bulk molecular gas, but in a low-metallicity regime where their outer layers are CO-deficient and CO-dark. The cloud masses, estimated from CO(3-2), range from 8.2×10^2 to $2.3 \times 10^4 M_\odot$. The most massive clouds appear similar to Orion A in SF activity as well as in gas mass. The common cloud mass structure also justifies the use of high-J CO transitions to trace the total gas mass of clouds, or galaxies, even in the high-z universe. This study is the first demonstration that CO(3-2) is an efficient tracer of molecular clouds even in low-metallicity environments. This study is published in the Astronomical Journal, entitled "First Detection of the Molecular Cloud Population in the Extended Ultraviolet (XUV) Disk of M83" by J. Koda, L. Watson, F. Combes, M. Rubio, S. Boissier, M. Yagi, D. Thilker, A. M Lee, Y. Komiyama, K. Morokuma-Matsui, and C. Verdugo.

Keywords. Interstellar medium (847), Molecular clouds (1072), Star formation (1569), Galaxy evolution (594), Spiral galaxies (1560), Galaxy disks (589)

1. Introduction

The GALEX satellite found massive star formation (SF) in the far outskirts of galactic disks (Gil de Paz et al. 2005; Thilker et al. 2005). Bright ultraviolet (UV) sources are distributed beyond the optical radius R_{25}. They reveal abundant and recent SF. These extended UV disks, dubbed XUV disks, are fairly common among local disk galaxies (Thilker et al. 2007). They offer an opportunity to study SF in extreme conditions, in particular, at a low average gas density and molecular fraction.

Molecular clouds host virtually all SF within the optical disks of local galaxies. It is crucial to study whether the same is true in XUV disks. Efforts have been made to detect CO emission there, however, they have rarely succeeded (Watson & Koda 2017, for review). Only four galaxies permitted CO detection at a few positions in their outskirts (Braine & Herpin 2004, Braine et al. 2007, Braine et al. 2010, Dessauges-Zavadsky et al. 2014). Most detections did not reveal individual clouds due to low sensitivity and resolution. Only M33, the closest to the Milky Way, allowed detection down to $\lesssim 4 \times 10^4 M_\odot$ in two regions beyond the R_{25} radius, and only one of them is identified as a single cloud (Braine et al. 2012). The rarity of the CO detection is at odds with the abundance of the UV sources across the XUV disks.

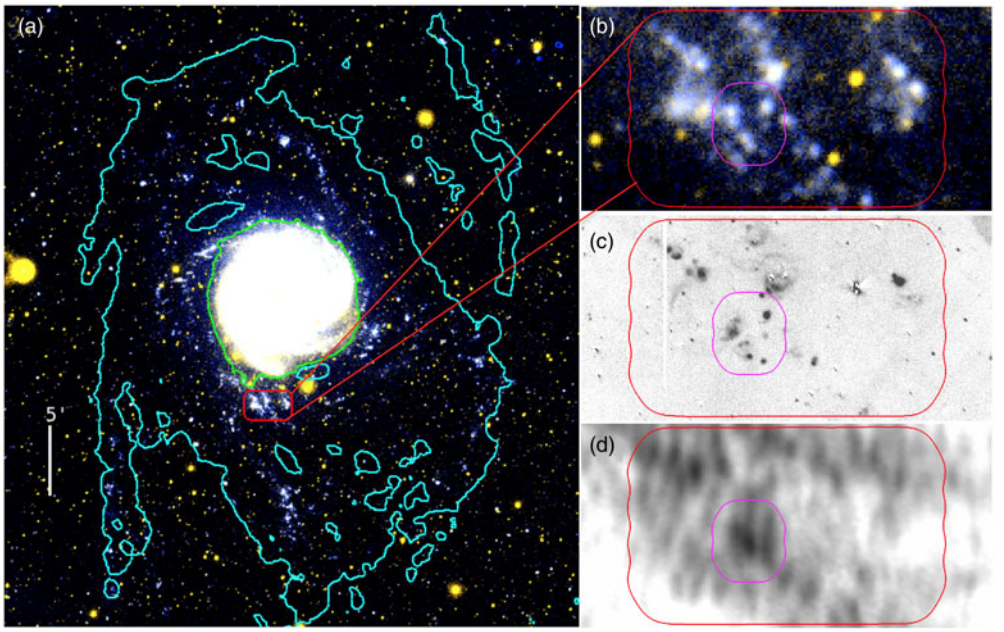

Figure 1. (a) GALEX FUV & NUV-band color composite image. The inner (green) and outer (cyan) contours are the edge of the optical disk and the extent of HI gas at an HI surface density of $1.5 \times 10^{20}\,\mathrm{cm}^{-2}$. The red box is the $1.5' \times 3'$ ($2.0 \times 3.9\,\mathrm{kpc}^2$) field from the ALMA CO(J=2-1) observations (Bicalho et al. 2019). The three panels on the right are zoom-in to the CO(2-1) field: (b) the GALEX color composite, as in Panel a; (c) the continuum-subtracted Hα image from the Subaru telescope, and (d) the HI 21cm emission image from Walter et al. (2008). The area of our CO(3-2) observations is indicated by the inner magenta box of $\sim 0.75' \times 0.85'$ ($\sim 0.98 \times 1.11\,\mathrm{kpc}^2$).

The previous ALMA observations of CO(2-1) in the XUV disk of M83 also resulted in non-detection even at a high mass sensitivity of $2.2 \times 10^4 \mathrm{M}_\odot$ (3σ; Bicalho et al. 2019). The observed field is a relatively large area of $\sim 1.5' \times 3'$ ($2 \times 4\,\mathrm{kpc}^2$) at a galactic radius of $r_{\rm gal} \sim 1.24 R_{25}$ with $R_{25} = 6.44'$ (8.4 kpc; Figure 1 red box).

2. ALMA CO(3-2) Observations and Detection of 23 Clouds

We revisit a smaller area of $\sim 0.75' \times 0.85'$ ($\sim 1\,\mathrm{kpc}^2$; Figure 1 magenta) within the CO(2-1) field (red) at a higher mass sensitivity by a factor of about 10 in CO(3-2) with ALMA. The target region is selected around the maximum HI 21 cm intensity position within the CO(2-1) observation. It includes bright UV peaks located at $\sim 1.24 R_{25}$ and is outside the traditional optical disk (green contour).

The new ALMA data clearly shows the detection of CO(3-2) emission (Figure 2). In the data cube, we identify pixels with $> 5\sigma$ peaks and find their envelopes by expanding their volumes to adjacent pixels down to 3σ significance. In some cases the edges of the 3σ envelopes of two peaks (two clouds) are connected. We use the CLUMPFIND algorithm (Williams et al. 1994) to split them – the partition of the two clouds is determined simply by assigning each pixel to the nearest of the two peaks. We visually inspect the results and manually merge them back to a single cloud when their intensity-weighted positions are closer than the beam size of 0.96" × 0.82". Figure 2 shows the IDs of the detected clouds.

The observed region has several HII regions (Figure 3). We visually identified significant Hα peaks in the Subaru Hα image. Panel a shows their locations. The Hα luminosity

https://doi.org/10.1017/S1743921322003684 Published online by Cambridge University Press

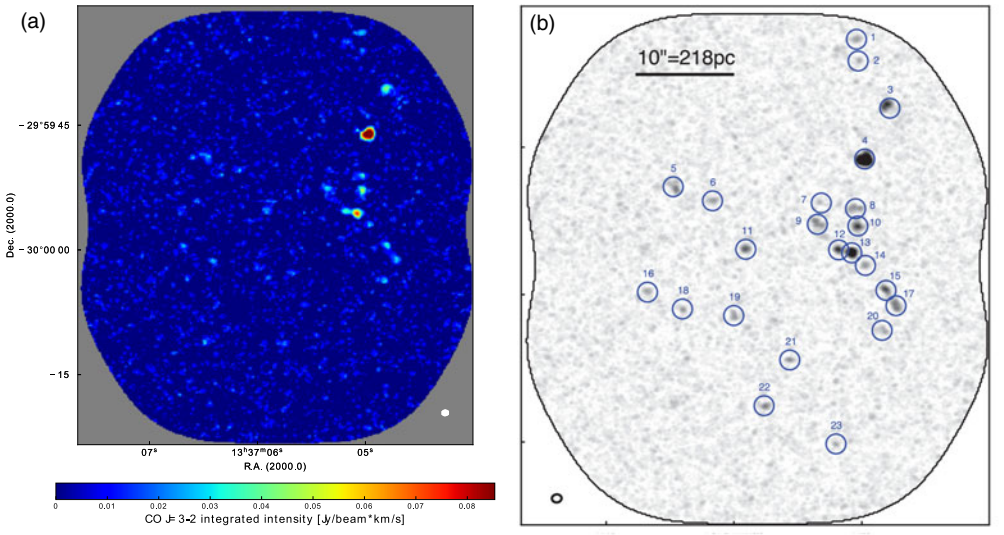

Figure 2. (a) CO(3-2) integrated intensity map. (b) Molecular clouds on the CO(3-2) peak intensity map. Each circle has a diameter of 2". The beam size of 0.96" × 0.82" (PA = −84.7 deg) is shown on the bottom-left corner, corresponding to 21×18 pc^2 at 4.5 Mpc.

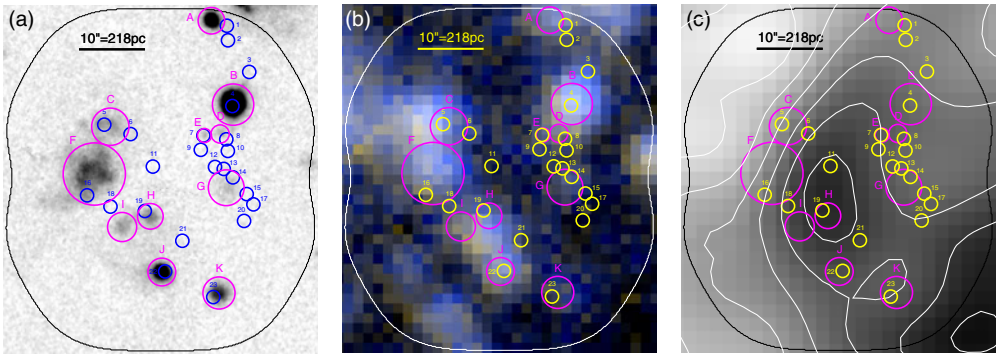

Figure 3. (a) Subaru H$_\alpha$ image at a resolution of about 1". (b) GALEX FUV & NUV-band color composite image at a resolution of about 5" (Gil de Paz et al. 2007b). (c) VLA+GBT HI 21cm image (grayscale) with contours – from the brightest – at 0.30, 0.25, 0.20, 0.15, 0.10, and 0.05 Jy/beam km s^{-1} with the 15" beam. The brightest contour corresponds to the HI surface density of $\sim 12 M_\odot$ pc^{-2} (and $\sim 16 M_\odot$ pc^{-2} for HI+He). Magenta circles denote the HII regions. Blue or yellow circles are molecular clouds and are the same as the ones in Figure 2.

($L_{\mathrm{H}\alpha}$) ranges from 1×10^{35} to 3×10^{37} erg s^{-1}. As a reference, in the Milky Way disk, the two HII regions in the Orion Nebula, M42 and M43, are located in the OMC-1 dense gas clump in the Orion A molecular cloud. They show $L_{\mathrm{H}\alpha} = 7.1 \times 10^{36}$ erg s^{-1} and 3.5×10^{35} erg s^{-1}, respectively (Scoville et al. 2001). Hence, our region has SF activity similar to, or slightly less than, that of the Orion Nebula, a relatively minor OB star forming region in the Milky Way.

3. Properties of the Detected Clouds

All clouds, except Cloud 4 and 8, are spatially unresolved; and Cloud 4 and 8 are only very marginally resolved at the resolution of 0.96" (21 pc). As a reference, the Orion

https://doi.org/10.1017/S1743921322003684 Published online by Cambridge University Press

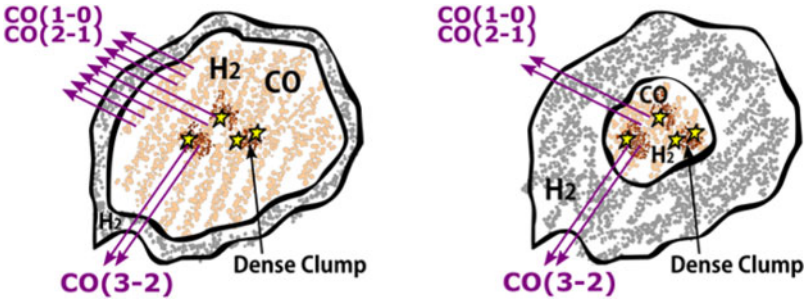

Figure 4. Schematic illustrations of the physical and chemical structures of a molecular cloud (a) in high-metallicity environment, and (b) in low-metallicity environment. The physical structures (i.e., mass distribution and SF activity) are common between (a) and (b), but their chemical structures (i.e., CO abundance) are different. The ambient radiation penetrates into the cloud, dissociates CO molecules in the cloud outer layers, and makes them CO-deficient and CO-dark, while more abundant H_2 molecules can self-shield themselves and remain (gray). These CO-dark layers thicken at low metallicity, since a lower dust abundance results in less efficient extinction and allows the radiation to penetrate deeper into the cloud (e.g., Maloney & Black 1988; van Dishoeck & Black 1988). Still, the CO molecules can remain near the cloud center (orange). We hypothesize that the dense clumps (brown), often associated with SF (yellow), are located at the heart of the cloud and likely remain intact with abundant CO molecules. The CO(3-2) emission originates from the dense clump region.

A cloud has a whole extent of ∼20 pc when it is observed in the CO(1-0) or CO(2-1) emission (Sakamoto et al. 1994; Nakamura et al. 2019; Kong et al. 2018). Its star-forming dense clump OMC-1 occupies only a small area (∼2pc) at the heart of the cloud and is bright in CO(3-2) (Ikeda et al. 1999). It is possible that our detected CO(3-2) peaks are mainly from dense clumps within molecular clouds, and hence, are unresolved.

The velocity dispersions of most clouds (σ_v) are resolved. Cloud 4 has a wide width of $\sigma_v = 6.1\,\mathrm{km\,s^{-1}}$ with a caveat that it could be a blend of two clouds. Again using Orion A as a reference, the velocity width of the bulk gas, measured in CO(1-0) and averaged over the whole cloud, is about $5\,\mathrm{km\,s^{-1}}$ at 50% of the peak brightness (from Figure 5 of Nakamura et al. 2019). The full CO(3-2) velocity width over the OMC-1 clump (size of about 2 pc) is not found in the literature; toward Orion KL (the brightest region), it is about $7\,\mathrm{km\,s^{-1}}$ at 50% of the peak brightness in a 134" (∼0.3pc) beam (from Figure 15 of Masui et al. 2021). Hence, the dense part has a broader linewidth than the entire cloud. These are similar to the velocity widths of Cloud 4 measured in CO(3-2).

For their measured σ_v, the XUV clouds generally have smaller (or similar) sizes compared to the clouds in the other galaxies. This makes sense if the CO(3-2) emission is primarily tracing dense clumps within the clouds, as seen in Orion A.

4. Hypothesis: Cloud Structure with Dense Clump and CO-dark Envelope

We are using the Orion A molecular cloud as a fiducial reference cloud given the similarity of its SF activity to the (brightest) clouds in the XUV disk. Orion A has an internal mass distribution common among other large and small Galactic molecular clouds, having small star-forming dense clump(s) embedded deeply in thick layers of bulk molecular gas (Nakamura et al. 1984; Enoch et al. 2008; Watanabe et al. 2017; Barnes et al. 2020). Figure 4a schematically illustrates this mass distribution. In terms of CO emissions, CO(1-0) and CO(2-1) can be excited easily at an average density and temperature in molecular clouds ($\sim 10^2\,\mathrm{cm^{-3}}$, $\sim 10\,\mathrm{K}$), and hence, the bulk gas contributes significantly to their total CO(1-0) and CO(2-1) luminosities (Kong et al. 2018;

https://doi.org/10.1017/S1743921322003684 Published online by Cambridge University Press

Nakamura et al. 2019). By having the J = 3 level temperature of $E_J/k \sim 33.2\,\mathrm{K}$ and critical density of $> 10^3\,\mathrm{cm}^{-3}$, the CO(3-2) emission requires higher density and temperature than the averages for excitation and is radiated predominantly from the dense clumps (Ikeda et al. 1999). Once it is excited in thermalized gas, CO(3-2) can become brighter than CO(1-0) and CO(2-1) in total flux. We hypothesize that the clouds in the XUV disk share the common clump-envelope mass distribution of the Galactic molecular clouds. The common mass structure is expected for gravitationally-bound clouds as it is determined predominantly by the internal physics rather than the environment.

Even when the mass distribution is the same, the chemical structure and appearance of the clouds in the CO emissions depend on the metal abundance (e.g., Maloney & Black 1988; van Dishoeck & Black 1988; Wolfire et al. 2010). In high metallicity ($\sim 1Z_\odot$; Figure 4a), the bulk gas in clouds can be detected in the low excitation transitions (J =1-0 or 2-1) of CO. In low metallicity ($< 1Z_\odot$), the dust extinction is low, and the ambient stellar radiation can penetrate deeper into the clouds. This radiation dissociates more CO in their outer layers through CO line absorptions, while the abundant H2 molecules can be self-shielded. This differential photo-dissociation makes the cloud outer layers CO-deficient and CO-dark while still H2-abundant (Figure 4b).

In our hypothesis, the dense clumps are protected from photo-dissociation and would radiate a similar amount of $L_{\mathrm{CO(3-2)}}$ in high and low metallicities. Hence, the calibration of cloud mass (M_{cloud})-to-$L_{\mathrm{CO(3-2)}}$ ratio in high metallicity should be applicable in low metallicity. The conversion equation from $L_{\mathrm{CO(3-2)}}$ to M_{cloud} derived in high metallicity (Wilson et al. 2009) can be used to estimate the cloud masses. This calculation provides a cloud mass range from $M_{\mathrm{cloud}} = 8.2 \times 10^2 \mathrm{M}_\odot$ to $2.3 \times 10^4 \mathrm{M}_\odot$. The maximum mass in this range is similar to the recently-estimated mass of the Orion A cloud ($4.0 \times 10^4 \mathrm{M}_\odot$; Nakamura et al. 2019).

JK acknowledges support from NSF through 25 grants AST-1812847 and AST-2006600.

References

Gil de Paz, A., Madore, B. F., Boissier, S., et al. 2005, ApJL, 627, L29
Thilker, D. A., Bianchi, L., Meurer, G., et al. 2007, ApJS, 173, 538
Watson, L. C., & Koda, J. 2017, in Outskirts of Galaxies, ed. J. H. Knapen, J. C. Lee, & A. Gil de Paz, Vol. 434, 175
Braine, J., & Herpin, F. 2004, Nature, 432, 369
Braine, J., Ferguson, A. M. N., Bertoldi, F., & Wilson, C. D. 2007, ApJL, 669, L73
Braine, J., Gratier, P., Kramer, C., et al. 2010, A&A, 520, A107
Dessauges-Zavadsky, M., Verdugo, C., Combes, F., & Pfenniger, D. 2014, A&A, 566, A147
Braine, J., Gratier, P., Contreras, Y., Schuster, K. F., & Brouillet, N. 2012, A&A, 548, A52
Bicalho, I. C., Combes, F., Rubio, M., Verdugo, C., & Salome, P. 2019, A&A, 623, A66
Williams, J. P., de Geus, E. J., & Blitz, L. 1994, ApJ, 428, 693
Scoville, N. Z., Polletta, M., Ewald, S., et al. 2001, AJ, 122, 3017
Sakamoto, S., Hayashi, M., Hasegawa, T., Handa, T., & Oka, T. 1994, ApJ, 425, 641
Nakamura, F., Ishii, S., Dobashi, K., et al. 2019, PASJ, 71, S3
Kong, S., Arce, H. G., Feddersen, J. R., et al. 2018, ApJS, 236, 25
Ikeda, M., Maezawa, H., Ito, T., et al. 1999, ApJL, 527, L59
Masui, S., Yamasaki, Y., Ogawa, H., et al. 2021, PASJ, 73, 1100
Nakamura, T., Kodaira, S., Ishii, K., Inatani, J., & Ohishi, M. 1984, PASJ, 36, 123
Enoch, M. L., Evans, II, N. J., Sargent, A. I., et al. 2008, ApJ, 684, 1240
Watanabe, Y., Nishimura, Y., Harada, N., et al. 2017, ApJ, 845, 116
Barnes, A. T., Kauffmann, J., Bigiel, F., et al. 2020, MNRAS, 497, 1972

https://doi.org/10.1017/S1743921322003684 Published online by Cambridge University Press

Maloney, P., & Black, J. H. 1988, ApJ, 325, 389
van Dishoeck, E. F., & Black, J. H. 1988, ApJ, 334, 771
Wolfire, M. G., Hollenbach, D., & McKee, C. F. 2010, ApJ, 716, 1191
Wilson, C. D., Warren, B. E., Israel, F. P., et al. 2009, ApJ, 693, 1736
Gil de Paz, A., Boissier, S., Madore, B. F., et al. 2007b, ApJS, 173, 185